# Bright monomeric photoactivatable red fluorescent protein for two-color super-resolution sptPALM of live cells

**Fedor V. Subach**[|], **George H. Patterson**[||], **Malte Renz**[|||], **Jennifer Lippincott-Schwartz**[|||], and **Vladislav V. Verkhusha**[|,*]

[|]Department of Anatomy and Structural Biology and Gruss-Lipper Biophotonics Center, Albert Einstein College of Medicine, 1300 Morris Park Avenue, Bronx, NY 10461

[||]Biophotonics Section, National Institute of Biomedical Imaging and Bioengineering, National Institutes of Health, 9000 Rockville Pike, Bethesda, MD 20892

[|||]Section on Organelle Biology, Cell Biology and Metabolism Program, National Institute of Child Health and Human Development, National Institutes of Health, 9000 Rockville Pike, Bethesda, MD 20892

## Abstract

Rapidly emerging techniques of super-resolution single-molecule microscopy of living cells rely on the continued development of genetically encoded photoactivatable fluorescent proteins. On the basis of monomeric TagRFP, we have developed a photoactivatable TagRFP protein that is initially dark but becomes red fluorescent after violet light irradiation. Compared to other monomeric dark-to-red photoactivatable proteins including PAmCherry, PATagRFP has substantially higher molecular brightness, better pH stability, substantially less sensitivity to blue light, and better photostability in both ensemble and single-molecule modes. Spectroscopic analysis suggests that PATagRFP photoactivation is a two-step photochemical process involving sequential one-photon absorbance by two distinct chromophore forms. True monomeric behavior, absence of green fluorescence, and single-molecule performance in live cells make PATagRFP an excellent protein tag for two-color imaging techniques, including conventional diffraction-limited photoactivation microscopy, super-resolution photoactivated localization microscopy (PALM), and single particle tracking PALM (sptPALM) of living cells. Two-color sptPALM imaging was demonstrated using several PATagRFP tagged transmembrane proteins together with PAGFP tagged clathrin light-chain. Analysis of the resulting sptPALM images revealed that single molecule transmembrane proteins, which are internalized into a cell via endocytosis, co-localize in space and time with plasma membrane domains enriched in clathrin light-chain molecules.

## 1. Introduction

Several super-resolution microscopy techniques, which provide spatial information below the diffraction limitation, are now available. However, techniques using precise molecular localization, such as photoactivated localization microscopy (PALM),[1] fluorescence photoactivated localization microscopy (FPALM),[2] stochastic reconstruction microscopy (STORM),[3] PALM with independent running acquisition (PALMIRA),[4] and stroboscopic PALM (SPALM)[5] have generated much interest. Although some of these techniques rely on

---

conventional fluorophores, most utilize photoactivatable organic dyes and genetically encoded fluorescent proteins (FPs).6 The photoactivatable FPs (PAFPs) are particularly useful for single particle tracking PALM (sptPALM), since it was developed to provide dynamic information about the spatial and temporal heterogeneity of the movement of individual molecules within a cell.7 Moreover, two-color sptPALM experiments should be very beneficial, since the relative dynamics of two proteins can be compared directly, and cell-to-cell variability becomes less problematic when discerning different phenotypes.

Several PAFPs have been described,8 however very few of them possess features that are optimal for the techniques mentioned above. An obligate tetrameric state of red PAFPs such as dark-to-red KFP1 (Ref.9) and green-to-red Kaede,10 EosFP,11 and IrisFP12 is incompatible with tagging of individual proteins due to potential protein aggregation artifacts. Currently available monomeric green-to-red PAFPs such as Dendra and Dendra2,13 tandem dimeric EosFP variant (tdEosFP),14 and enhanced mEos2 (Ref.15), exhibit bright green fluorescence before photoconversion. The original green fluorescence in these PAFPs complicates their use in two-color photoactivation experiments with green PAFPs, such as irreversibly photoactivatable dark-to-green PAGFP16 and cyan-to-green PSCFP17, and reversibly photoswitchable dark-to-green mTFP0.7 (Ref.18) and Dronpa19. Incomplete green-to-red photoconversion is a further complication, especially for two-color PALM. Reversibly photoswitchable dark-to-red PAFPs rsCherry and rsCherryRev could be used in two-color experiments with green PAFPs, but have low brightness in their On state, suffer from low contrast, and spontaneously relax back to the dark state.20 The available PAmRFP1 (Ref.21) protein and its improved variant PAmCherry1 (Ref.22) are both derived from DsRed. They irreversibly photoconvert from a dark to a red state after illumination with violet light. PAmRFP1, however, lacks the photon yield required for PALM applications. PAmCherry1 is brighter than PAmRFP1 but is still not as bright as permanently red FPs such as TagRFP.23 This is a limitation for its application in cell imaging in ensemble mode such as widefield and confocal microscopy. In addition, PAmCherry1 produces enough photons to enable a PALM image but 80% of fluorescence gets photobleached within 2–3 frames.22 PAmCherry1 thus is not optimized for photostability, a key property for use in sptPALM.

In this paper, we applied structure-based rational and random mutagenesis to the TagRFP protein in order to convert it into a bright irreversibly photoactivatable red FP, named PATagRFP. We also demonstrated the utility of PATagRFP as a photoactivatable red probe for tracking trajectories of single molecules in live cells using a two-color sptPALM imaging.

## 2. Experimental Procedures

### 2.1. Mutagenesis and screening of libraries

TagRFP[23] and PAGFP[16] genes were amplified as the *Bgl*II-*Eco*RI fragments using polymerase chain reaction and inserted into a pBAD/His-B vector (Invitrogen). Site-specific mutagenesis of TagRFP was performed using a QuickChange Mutagensis Kit (Stratagene). For simultaneous mutagenesis at several positions, an overlap-extension approach was applied.[24] Random mutagenesis was performed with a GeneMorph II Random Mutagenesis Kit (Stratagene) using conditions that resulted in the mutation frequency of up to 16 mutations per 1000 base pairs. After the mutagenesis, a mixture of mutated genes was electroporated into LMG194 bacterial host cells (Invitrogen).

Libraries of $10^6$–$10^7$ independent clones of TagRFP mutants were photoactivated with a custom built 405/20 nm LED array (50 mW/cm$^2$) and screened using a MoFlo (Dako) fluorescence-activated cell sorter (FACS), followed by colony visualization using a Leica MZ16F fluorescence stereomicroscope, as previously described.[22] After each round of the

FACS screening, typically 20–40 best photoactivatable candidate clones were sequenced, purified, and characterized before the next round of mutagenesis.

## 2.2. Characterization of the purified proteins

PAGFP, PAmCherry1, TagRFP and PATagRFP mutant proteins with polyhistidine tags were expressed in LMG194 cells grown overnight in RM medium supplemented with 0.002% arabinose at 37°C, and then purified using a Ni-NTA agarose (Qiagen). For spectroscopy, photoactivation of purified proteins was performed with a 405/20 nm LED array (~50 mW/ $cm^2$) in a 50 μl quartz microcuvette (Starna Cells) at a room temperature. The excitation and emission spectra of recombinant proteins were measured with a FluoroMax-3 spectrofluorometer (Jobin Yvon). For absorbance measurements, a Hitachi U-3010 spectrophotometer was used.

To determine extinction coefficients, we relied on measuring the mature chromophore concentration. For that, the purified proteins were alkali-denatured. It is known that extinction coefficient of the tyrosine-containing GFP-like chromophores is 44,000 $M^{-1}cm^{-1}$ at 447 nm in 1 M NaOH.[17] Based on the absorbance of the native and denatured proteins, molar extinction coefficients for the native states were calculated. For determination of quantum yields, fluorescence of the photoactivated mutant variants was compared with an equally absorbing Rhodamine-101 dye dissolved in ethanol containing 0.01% HCl (quantum yield is close to 1.00 (Ref.25)). Photoactivation contrast was determined as a ratio of the areas under the fluorescence emission spectra before and after the protein photoactivation. The pH titrations were performed using a series of buffers (100 mM NaOAc, 300 mM NaCl for pH 2.5–5.0, and 100 mM $NaH_2PO_4$, 300 mM NaCl for pH 4.5–10.5).

The photobleaching kinetics was measured using the purified protein at concentrations of 1 mg/ml in aqueous (phosphate buffered saline, PBS) drops in oil using Olympus IX81 inverted microscope equipped with a 200 W metal-halide lamp, a 100× 1.4 NA oil objective lens, 570/30 nm excitation and 615/40 nm emission filters, and neutral density filters (11.8 and 30.7% transmission). The microscope was operated with a SlideBook 4.1 software (Intelligent Imaging Innovations). Light power densities were measured at a rear aperture of the objective lens. The photoactivation kinetics was measured using the above conditions with the neutral density filters of 2.9, 11.8, 21.4, 30.7, 41.1, 52.9, 71.8 and 78.5% transmission, and either the 350/50 or 390/40 nm filters for photoactivation. All data were normalized to spectral output of the lamp, transmission profiles of the filters and dichroic mirror, and absorbance spectra of the respective proteins.

The dependences of maximal fluorescence intensities and photoactivation rates on the photoactivation wavelengths were measured using the same conditions as described for the photobleaching kinetics, except a monochromator (Jobin Yvon) with a 20 nm bandwidth and a 150 W xenon lamp was used as the excitation light source. Light from the monochromator was directed into the light-guide using a 20× 0.5 NA UPlanFL objective lens (Olympus). The maximal fluorescence intensity corresponded to the maximal value (i.e., the plateau) on the photoactivation curve. The maximal photoactivation rate corresponded to the maximum value on the curve, resulting from a differentiation of the photoactivation curve.

To study protein maturation, LMG194 bacteria were grown at 37°C overnight in RM medium supplemented with ampicillin. Next morning cells were diluted to optical density 1.0 at 600 nm, and 0.2% arabinose was added. Upon induction of protein expression, the bacterial cultures were grown at 37°C in 50 ml tubes filled to the brim and tightly sealed to restrict oxygen availability. After 2 hours, the cultures were centrifuged in the same tightly closed tubes. After opening the tubes, the proteins were purified using the Ni-NTA resin within 30 min, with all procedures and buffers at or below 4°C. Protein maturation occurred in PBS at 37°C; and red

fluorescence of the protein aliquots photoactivated at each time point was monitored using the FluoroMax-3 spectrofluorometer.

## 2.3. Mammalian plasmids and cell culture

To construct pPATagRFP-C1, pPATagRFP-β-actin and pPATagRFP-α-tubulin plasmids, the PATagRFP gene was PCR amplified as a *Nhe*I-*Bgl*II fragment with the -GGGG- linker at the C-terminus and swapped with the EGFP gene in the pEGFP-C1, pEGFP-Actin and pEGFP-Tubulin vectors (Clontech), respectively. To design pPATagRFP-H2B plasmid, the PATagRFP gene was swapped with the PAmCherry1 gene in the pPAmCherry1-H2B plasmid. [22] To generate pTfR-PATagRFP and pVSVG-PATagRFP plasmids, a PCR-amplified *Bam*HI-*Not*I fragment encoding the PATagRFP gene was swapped with the mCherry or mEGFP genes in the pTfR-mCherry1 and pVSVG-mEGFP plasmids, respectively.[22] To construct pPATagRFP-N1 plasmid, the PATagRFP gene was PCR amplified as a *Age*I-*Bsr*GI fragment with deletion of the *Bsr*GI site in the N-terminal part and swapped with the EGFP gene in the pEGFP-N1 vector (Clontech). To generate pEGFR-PATagRFP plasmid, a *Sac*II-*Bsr*GI fragment containing the PATagRFP gene was cut out from the pPATagRFP-N1 plasmid and was swapped with the mRFP1 gene in the pEGFR-mRFP1 plasmid.[26]

HeLa and COS-7 cells were grown in Dulbecco's Modified Eagle Medium containing 10% fetal bovine serum and 2 mM glutamine (Invitrogen). Cells were grown in Lab-Tek chambers with #1.0 borosilicate coverslips in the bottom (Nalge Nunc) or on #1.0 25 mm round coverslips (Warner Instruments). Plasmid transfections were performed with a FuGENE-6 transfection reagent (Roche). Live cells were photoactivated and imaged in a dye-free DMEM medium without serum (Invitrogen).

## 2.4. Fluorescence microscopy and cell imaging

Widefield imaging of live cells was performed 48–72 h after transfection. Cells were imaged using the Olympus IX81 inverted microscope equipped with a 100× oil objective, a 200 W metal-halide lamp, a 390/40 nm exciter for photoactivation, and a filter set (570/30 nm exciter, 615/40 nm emitter) (Chroma) to acquire red fluorescence.

sptPALM imaging of single molecules was performed at 37°C on an Olympus IX81 microscope using a 60× 1.45 NA PlanApoN TIRF objective (Olympus), as previously described[1,7] with the exception that a DualView Imaging System (Photometrics) was used for the two-color PALM imaging. Lasers used for excitation were a 50 mW 561 nm (CrystaLaser), a 50 mW 488 nm Sapphire (Coherent), and a 50 mW 405 nm CUBE (Coherent). Power levels, measured near the rear aperture of the objective lens, ranged 0.1–0.25 mW (estimated <60 W/cm$^2$ at the sample) for the 561 nm laser, 0.1–0.25 mW (estimated <60 W/cm$^2$ at the sample) for the 488 nm laser, and <25 TW (estimated <2.5 W/cm$^2$ at the sample) for the 405 nm laser. Fluorescence was detected with an iXon EMCCD camera (Andor Technology). Image analysis was performed as previously described.[1] Coverslips were cleaned with 1% hydrofluoric acid or piranha wash as previously described.[27] Gold beads (50 nm or 100 nm diameter) and tetraspecks (Invitrogen) were used as fiduciary markers.

# 3. Results

## 3.1. Development of photoactivatable TagRFP variants

Recently reported TagRFP[23] is the brightest monomeric red FPs currently available. This prompted us to use TagRFP as an initial template for developing a bright monomeric red PAFP variant. Based on the crystal structure of the TagRFP's far-red derivative known as mKate[28] and mutations observed in the PAmCherry variants,[22] we have identified amino acids at the positions 69, 84, 148, 165, 167, 181 and 203 (numbering follows the alignment with GFP, see

Figure 1), which could be crucial for the photoactivation of a chromophore. We performed simultaneous mutagenesis of TagRFP at these positions. A bacterial library of the mTagRFP mutants with a size of ~$10^6$ independent clones was screened with the FACS after illumination with 405 nm LED array, followed by selection of colonies on Petri dishes using the fluorescence stereomicroscope. The Petri dishes were photographed twice, before and after the illumination with 405 nm LED array; and the brightest colonies exhibiting the largest photoactivation changes from dark to red were selected. We have found first eight photoactivatable TagRFP variants containing combinations of different substitutions at the mutated positions such as 69S,K,N,Q, 84W, 148N,S,H,L,T,F, 165S,A,V,G,L,Q, 167M,G, 181F,L, and 203R. These variants had the highest photoactivation contrast and brightest red fluorescence in the photoactivated state, as compared to other mutant clones. To further improve these properties, we subjected these variants to three rounds of random mutagenesis. After each round, 250 clones with improved properties were sequenced, purified, and spectroscopically characterized in an ensemble mode. After the third round of screening, we selected two variants, PATagRFP1297 and PATagRFP1314, for a detailed characterization (Table 1).

A semi-native gel analysis of the purified PATagRFP1297 and PATagRFP1314 proteins indicated, however, that they formed oligomers, as observed for TagRFP (Supporting Figure 1). Furthermore, the PATagRFP1297 and PATagRFP1314 fusions with α-tubulin, expressed in mammalian cells and imaged after photoactivation, only partially incorporated into endogenous structures, formed cytoplasmic aggregates, and had a high intracellular fluorescent background. Analysis of the structure of mKate, which was crystallized as a tetramer, indicated that the surfaces of protein subunits develop two types of interfaces: IF1 and IF2.[28] The IF1 interface was noticeably weaker compared to IF2. Based on interactions observed in the latter interface, we introduced M151K, Y153K and C229S mutations to break IF2 in PATagRFP1297. The amino acids at positions 162 and 164 were also converted back to those observed in TagRFP. The resulting PATagRFP1297/M151K/Y153K/E162G/V164R/C229S variant was named PATagRFP. The five new mutations served to block the formation of dimers and oligomers of PATagRFP in vitro (Supporting Figure 1) and resulted in its monomeric behavior in vivo. Indeed, the β-actin, α-tubulin and histone H2B fusions with PATagRFP produced properly localized molecules in living HeLa cells (Supporting Figure 2). Thus, the final PATagRFP protein contained 12 substitutions in the parental TagRFP sequence: R69S/F84W/Q139K/A147P/N148S/M151K/Y153K/S165V/H203R/R207I/V218W/C229S (Figure 1).

### 3.2. Spectral and biochemical properties of PATagRFP

Before photoactivation, no substantial absorbance of PATagRFP was detected at wavelengths above 300 nm. After photoactivation, using the 405/15 nm LED array, an absorbance peak developed with a maximum at 562 nm (Figure 2A). In the photoactivated state, the PATagRFP exhibited red fluorescence with the excitation/emission peaks at 562/595 nm, respectively (Figure 2A). Molar extinction coefficient and quantum yield of the photoactivated PATagRFP protein were 66,000 $M^{-1}cm^{-1}$ and 0.38, respectively (Table 1). Thus, PATagRFP has 3- and 1.9-fold greater brightness than PAmCherry1[23] and common ECFP, respectively, and only 1.3-fold lower brightness than common EGFP, that makes it the brightest dark-to-red monomeric PAFP (Table 1). The red state of PATagRFP was stable with time, indicating that the photoconversion reaction was irreversible. Maturation half-time for PATagRFP was 75 min at 37°C (Table 1), which is 1.2-fold faster than that of parental TagRFP. The photoactivation fluorescence contrast achieved with the purified PATagRFP protein was ~540-fold. The PATagRFP fluorescence exhibited higher pH stability than that of PAmCherry1 and other monomeric red PAFPs (Table 1) with the apparent $pK_a$ value of 5.3 (Figure 2B). The high pH stability makes PATagRFP useful as a potential tag for intracellular proteins localized in acidic compartments.

At a relatively high intensity of photoactivation light in a widefield microscope (50 mW/$cm^2$; unless specifically stated, here and below the light power density is measured at a rear aperture of the 100× oil objective lens) PATagRFP had 2.4- and 5.1-fold slower photoactivation kinetics than that for PAmCherry1 and PAGFP, respectively (Figure 2C). Decreasing power of the photoactivation light reduced the difference in the photoactivation half-times for these proteins (Figure 2D). At the lowest tested power of the photoactivation light (5.9 mW/$cm^2$) PATagRFP and PAGFP demonstrated rather similar photoactivation half-times (Figure 2D).

At a relatively high intensity of the photobleaching light (82 mW/$cm^2$) at the widefield microscope, red fluorescence of PATagRFP photobleached 1.2- and 5.9-fold slower than that of PAmCherry1 and TagRFP, respectively (Figure 2E). The difference in photostability between PATagRFP and TagRFP reduced with the decreasing power of the photobleaching light (Figure 2F). At the lowest tested (9.6 mW/$cm^2$) PATagRFP was 1.8- and 2.9-fold more photostable than PAmCherry1 and TagRFP, respectively.

### 3.3. Photochemical properties of PATagRFP in ensemble

Maximal efficiencies of photoactivation for the purified PATagRFP, PAmCherry1 and PAGFP proteins were observed at about (400–420)± 10 nm, 400±10 nm, and (380–400)± 10 nm, respectively (Figure 3A). These maxima coincided with an absorbance peak at 405 nm observed for PAmCherry1 in a dark state, and with a 412 nm absorbance peak attributed to an intermediate detected in the process of the PATagRFP photoactivation (Figure 3B). The photoactivation efficiency for PATagRFP, PAmCherry1 and PAGFP dropped dramatically with the increasing photoactivation wavelength above 420 nm (Figure 3A). For example, during the same photoactivation time as maximal efficiencies, the 480±10 nm blue light photoactivated only 14%, 4% and 1% of the PAmCherry1, PATagRFP and PAGFP molecules, respectively. It is important to note that 3.5-fold decrease in the efficiency of the PATagRFP photoactivation with blue light, as compared to PAmCherry1, represents the obvious advantage of PATagRFP over PAmCherry1 for two-color photoactivation and PALM experiments with green PAGFP, imaged using a 488 nm laser.

In the process of the PATagRFP photoactivation, a temporary band at 412 nm was detected (Figure 3B). The maximum of the 412 nm intermediate form was observed ~5 min after the beginning of the photoactivation using a low 405/15 nm light power (50 mW/$cm^2$ at the protein sample) and completely disappeared by 60 min of the light illumination. The maximal absorbance of the intermediate was 50-fold lower than that of the 562 nm peak corresponding to the photoactivated PATagRFP. During photoactivation, a 339 nm absorbance peak appeared and increased during the whole 60 min activation period. It has been suggested that 330–340 nm absorbance band corresponds to the red chromophore observed in DsRed,[29] mCherry,[30] mKate[31] and PAmCherry1.[22] Interestingly, the highly concentrated PATagRFP sample (27 mg/ml) in its dark state showed a very weak absorption at ~351 nm (Figure 3B, insert), but the protein did not fluoresce when excited at this wavelength.

The dependence of the initial photoactivation rate of PATagRFP on the wavelength of photoactivation light had maxima at 360±10 nm and 400±10 nm (Figure 3C). These maxima were close to the 351 nm and 412 nm absorbance peaks. We hypothesized that the PATagRFP photoactivation starts from the 351 nm initial dark form, which photoconverts into the 412 nm temporal intermediate, which in turn photoconverts into the 562/595 nm red form. That pathway might explain the ~2-fold slower PATagRFP photoactivation kinetics observed with 390/40 nm light comparing to PAmCherry1 (Figures 2C,D). To test this hypothesis, we first compared photoactivation characteristics of PATagRFP achieved with 390/40 nm light with those registered with 350/50 nm light. The 390/40 and 350/50 nm light bands should selectively affect either 351 nm absorbing form or 412 nm absorbing intermediate, respectively. Indeed, the 350/50 photoactivation light resulted in the accumulation of the 412 nm intermediate and

increased the maximal yield of its formation ~5-fold as compared to the photoactivation with the 390/40 nm light (Figure 3D).

We next checked whether the 390/40 nm light is required for converting the 412 nm intermediate into the red form. After illumination of PATagRFP with 350/50 nm light for 1 min, we placed the protein sample either in the dark or subjected it to irradiation with the 390/40 nm light (Figure 3E). The 412 nm intermediate converted into the red form in the darkness with the transition half-time of 34 min, according to the fluorescence of the red form. However, illumination with the 390/40 nm light accelerated the transition half-time more than 500-fold (Figure 3E, insert). Intensity dependence of PATagRFP photoactivation was determined by illuminating the dark protein sample using different powers of the 350/50 nm light. The 350/50 nm light was selected to affect the 351 nm absorbing form. The initial rates of the PATagRFP photoactivation had a linear dependence on the light power with a slope of 2.2±0.2 (Figure 3F), suggesting that photoactivation required absorption of two photons. We concluded that the PATagRFP photoactivation is a two-step photochemical process involving one-photon absorbance by two distinct chromophore forms.

### 3.4. Single-molecule evaluation of PATagRFP variants

For PALM characterization, PATagRFP1297, PATagRFP1314, PATagRFP and PAmCherry1 were tagged to the vesicular stomatitus virus G protein tsO45 (VSVG).[32] The VSVG chimeras trafficked to the plasma membrane, making them amenable to imaging by total internal reflection fluorescence (TIRF) microscopy. Live COS-7 cells expressing the chimeras were imaged in sptPALM experiments under the low levels of 561 nm excitation and 405 nm photoactivation, and were monitored for morphological changes before and after the experiment. Single-molecule statistics indicated that all three PATagRFP variants were more photostable than PAmCherry1 (Figure 4A). The PATagRFP1297 and PATagRFP1314 proteins were most photostable but were not utilized for further experiments due to their oligomerization tendencies described above. Compared to PAmCherry1, monomeric PATagRFP was 1.3-fold more photostable in cells and showed 3-fold more molecules lasting ≥0.7 sec (i.e., after 7 frames) (Figure 4B). A higher PATagRFP photostability was also observed in ensemble studies (Figure 2F). PATagRFP molecules emitted 1.5-fold more photons per frame (Figure 4C) and had similar sigma per frame as PAmCherry1 (Figure 4D).

### 3.5. Two-color sptPALM characterization of transmembrane proteins

For further sptPALM experiments, PATagRFP was fused to epidermal growth factor receptor (EGFR),[33] and VSVG was fused with dark-to-green PAGFP. We then co-expressed both transmembrane chimeric molecules, EGFR-PATagRFP and VSVG-PAGFP, in COS 7 cells (Figure 5). PALM live cell imaging demonstrated a punctate distribution of both chimeras throughout the plasma membrane (Figures 5A, D). A merged image indicated a partial colocalization of VSVG and EGFR molecules within the same punctate regions (Figures 5G; see arrows), but the majority of clusters appeared to contain one transmembrane chimera and not the other. The tracking of molecules lasting >0.7 second showed movement of 1635 VSVG-PAGFP and 627 EGFR-PATagRFP molecules throughout the membrane. This analysis also revealed few of the two chimeras within the same cluster and even in the areas of overlapping in the plots of all molecules, the tracks lasting >0.7 second did not overlap in the temporal domain (Figure 6). Thus, it is unclear whether they sampled the same cluster at different times or if different clusters were formed over the course of the experiment.

Two-color sptPALM was also performed using transmembrane chimeras with transferrin receptor (TfR)[34] (Supporting Figures 3, 4), EGFR (Supporting Figures 5, 6), and VSVG (Supporting Figures 7, 8) in concert with a clathrin light chain (CLC)[35] tagged with PAGFP (PAGFP-CLC). Since CLC is part of the clathrin-coated pit machinery, it offers a good marker

for clathrin-coated pits, distinct membrane domains into which some plasma membrane proteins are internalized for endocytosis. Although their mechanisms may differ, both TfR and EGFR proteins have signal peptide sequences that promote efficient endocytosis via clathrin-coated pits,36 while the VSVG protein has an inefficient clathrin mediated internalization signal.37 Two-color sptPALM images are shown for TfR-PATagRFP (Supporting Figures 3A,D,G), EGFR-PATagRFP (Supporting Figures 5A,D,G), and VSVG-PATagRFP (Supporting Figures 7A,D,G). They demonstrate punctate regions for all proteins distributed throughout the plasma membrane, with some CLC pits overlapping with TfR and EGFR clusters, but very few with VSVG.

Clathrin light chain exchanges between clathrin coated pit bound and free forms. The free cytoplasmic PAGFP-CLC diffusion is likely too rapid to monitor with the ~9.4 per second frame rate used in these experiments, so detection and analysis of the PAGFP-CLC molecules is likely to be limited to those bound to clathrin-coated pits. The tracking analysis for PAGFP-CLC showed these molecules in distinct domains located throughout the surface of the cell (Supporting Figures 3B, 5B, 7B). Diffusion maps in Supporting Figures 3C, 5C, 7C indicate that PAGFP-CLC is largely immobile when localized in these domains. The transmembrane chimeras TfR, EGFR, and VSVG also showed tracks located throughout the cell membrane (Supporting Figures 3E, 5E, 7E), and these had a notable range of diffusion coefficients (Supporting Figures 3F, 5F, 7F).

One application of the two-color sptPALM method is to study dynamics of various molecules within and around distinct membrane domains. Overlays of the PAGFP-CLC tracks with those of TfR-PATagRFP (Supporting Figures 3H,I) and EGFR-PATagRFP (Supporting Figures 5H,I) showed examples of the overlap between domains, whereas examples of overlap with VSVG-PATagRFP were less common (Supporting Figures 7H,I). Approximately, 3% of TfR molecules and ~4.5% of EGFR molecules imaged were found to diffuse into or within formed PAGFP-CLC domains over the course of the experiments, whereas <1% of VSVG molecules was found within these domains. Since, these are live cell experiments over ~15 minute period, during which a cell can move and domains can move, disperse, and reform, we also analyze these data as a function of time to check the localization of chimeric molecules within the same area at the same time. In the examples where an overlap of tracks from PAGFP-CLC was observed with those of TfR-PATagRFP and EGFR-PATagRFP, these overlaps were found to occur in the temporal dimension also (Supporting Figures 4, 6). In contrast, a similar three-dimensional plot for PAGFP-CLC and VSVG-PATagRFP showed little overlap of the tracked molecules and the CLC domains even in areas that appeared colocalized in the 2D tracks (Supporting Figure 8).

## 4. Discussion

Previous work using photoswitchable green-to-red tandem dimeric tdEosFP as a photoactivatable probe indicated that it worked well for single-color sptPALM.[7] The use of tdEosFP in two-color sptPALM, however, is complicated by the bright green fluorescence that tdEosFP exhibits before photoactivation. Although it does not preclude its use in two-color PALM imaging,[27] the entire data set for each fluorophore must be collected sequentially. In that case, the two-color sptPALM experiments may be performed similarly but this will lead to a large time difference between collections of the data for the two molecules. We developed PAmCherry1 for the two-color PALM experiments[23] because its lack of any pre-photoactivation fluorescence results in minimal overlap in fluorescence signal with its green PAFP partner. While PAmCherry displayed a good photoactivation contrast and localization precision compared to tdEosFP, when tagged to molecules of interest PAmCherry1 was less photostable than tdEosFP, making it less useful for sptPALM in live cells. To improve

PAmCherry1, we thus designed a brighter and more photostable version, called PATagRFP, useful in both two-color PALM as well as sptPALM.

## 4.1. Mutations observed in PATagRFP

We have identified 12 amino acid mutations present in PATagRFP, as compared to the parental TagRFP (Figure 1). Among them R69S, F84W, N148S, S165V, H203R, R207I, and V218W are internal to the TagRFP β-can protein fold, while Q139K, A147P, M151K, Y153K and C229S are external to the fold. An irreversibly photoactivatable mutant with a minimal number of mutations contained R69S, F84W and H203R substitutions. It has been shown that positively charged side chains of Lys or Arg at the position 69 are important for the formation of the red chromophore in DsRed,[38] fluorescent timers[39], and mCherry.[30] However, the effect of these residues can be substituted with a positively charged amino acid at the spatially close position 203, as it has been observed in Rtms5 and its derivatives,[40] mKeima[41] and PAmCherry1.[42] It has been also shown that the K69N and I203R mutations are minimally required to convert mCherry into a red PAFP variant.[22,42] Crystallographic analyses of PAmCherry1 (Ref.[42]) and the TagRFP's derivative mKate,[28] indicate that positions 69 and 203 are located close to the Tyr66 $C^{\alpha}$–$C^{\beta}$ double bond of the red chromophore and may participate in its formation. It has been also suggested that positively charged amino acids at positions 69 and 203 are necessary to maintain the catalytic Glu222 residue as an anion and/or to serve as a general base for proton abstraction during oxidation of the Tyr66 $C^{\alpha}$–$C^{\beta}$ bond.[42,43]

In several red FPs, hydrophobic amino acids Leu, Phe and Trp at position 84 are important for the formation of neutral chromophore forms that absorb at 400–410 nm and have been suggested to be intermediates in the red chromophore pathway.[44,45] According to the crystal structure of mKate, the residues at positions 148 and 165 form hydrogen bonds with the hydroxyl group of Tyr66 of the chromophore in its *cis-* and *trans-*configurations, respectively.[28] These hydrogen bonds appear to be important for stabilizing the *cis-* and *trans-*configurations and for maintaining the anionic state of the chromophore. Consequently, the N148S and S165V substitutions in the PATagRFP protein favor the formation of the *cis* chromophores, such as those observed in mKate[28] and mCherry.[46] The V218W substitution in PATagRFP decreased the photoactivation contrast 1.6-fold but notably increased the protein's photostability and brightness. In mKate, bulky Trp218 is close to Gln220 and can influence the positioning of this residue.[28] It was suggested that Gln220 can affect the formation of N-acylimine in the chromophore of the DsRed/Q65M variant.[47] In addition, the R207I substitution slightly improved brightness and contrast of PATagRFP. According to the mKate structure, Arg207 is in a close proximity to Trp218, suggesting that the R207I mutation provided better fitting of a bulky Trp218 within the protein environment. An external mutation A147P increased both contrast and brightness of PATagRFP by 9-fold and 1.7-fold, respectively. The A147P mutation may influence the positioning of the adjacent Ser148, which has been suggested to make a hydrogen bond with the chromophore phenolate. An external mutation Q139K possibly improved maturation and protein folding. Other external mutations, such as M151K, Y153K, and C229S, were required to maintain PATagRFP in its monomeric state by disrupting the hydrophobic interface IF2. Lastly, the C229S substitution at the C-terminus of PATagRFP should prevent the formation of intermolecular S-S bonds.

## 4.2. Photoactivation of PATagRFP

Due to a high similarity between PATagRFP and PAmCherry1 observed in their: (i) internal substitutions relative to the parental TagRFP and mCherry proteins, and (ii) photoactivation phenotypes (Figure 2) we hypothesized that they may have had similar photoactivation pathways.[42,45] However, our spectroscopic analysis (Figure 3) suggests that the initial dark states in PATagRFP and PAmCherry1 are different. Whereas PAmCherry1 in the dark state has a pronounced absorbance peak at 404 nm,[22] the PATagRFP's initial dark state absorbs at

substantially shorter wavelength of 351 nm; and, similar to the PAmCherry's dark state, 412 nm absorbance peak only temporarily appears during the process of the PATagRFP photoactivation. It has been also shown that blue-emitting mutants of the TagRFP, mCherry, HcRed1, M355NA, mKeima red FPs,[44] and autocatalytically converting from a blue to the red states fluorescent timer FPs[39] all have the 400–410 nm absorbing states, which correspond to the neutral forms of the chromophores. The crystal structure and mass-spectrometry analysis of PAmCherry1 in the dark state revealed that its chromophore represents an N-acylimine group conjugated with the cyclized 65–67 tripeptide, with a single non-oxidized $C^\alpha$-$C^\beta$ bond in the Tyr66 side chain.[42] The PAmCherry1 photoactivation caused the formation of a $C^\alpha$-$C^\beta$ double bond in the Tyr66 side chain that resulted in an extension of the chromophore conjugation.

We hypothesized that, since the 351 nm PATagRFP form is a predecessor of the 412 nm form, it may represent a cyclized dehydrated aromatic α-enolate without the N-acylimine and without the oxidized Tyr66 $C^\alpha$-$C^\beta$ bond (Scheme 1). It has been suggested that the α-enolate intermediate is formed at early stages of the chromophore maturation in FPs.[48] Furthermore, a GFP mutant having the Ala65-Phe66-Gly67 chromophore tripeptide and the E222A mutation had a single absorbance peak at ~360 nm.[49] Its crystal structure has revealed that the resulting chromophore represented the cyclized dehydrated α-enolate moiety.[49] In PATagRFP, the α-enolate moiety absorbing at 351 nm possibly photoconverts into the 412 nm absorbing form with a chemical structure similar to that of the dark chromophore in PAmCherry1.[42] Further photoconversion of the 412 nm form into the red fluorescent state is accelerated >500-fold by illumination with a 390/40 nm light (Figure 3E); and the overall PATagRFP photoactivation is a two-photon process (Figure 3F). Therefore, we suggest that absorbance of the second photon by the 412 nm intermediate converts PATagRFP into the final red fluorescent state (Scheme 1).

## 4.3. PATagRFP in two-color sptPALM

In addition to developing PATagRFP as a much brighter red PAFP for conventional fluorescence imaging, we tested PATagRFP as a photoactivatable PALM probe in cells with chimeras of three transmembrane proteins localized on the plasma membrane. These data indicated that it would indeed function as a better sptPALM probe than PAmCherry1 by providing ~3 times more molecules per experiment with our track-length cutoff of >0.7 second. Using PATagRFP as the marker in partner with PAGFP, we followed TfR, EGFR, and VSVG by 2-color sptPALM. All have populations on the plasma membrane, but TfR and EGFR differ from VSVG by having signal sequences that can efficiently target them to clathrin-coated pits during endocytosis. Since their ligands promote rapid internalization of the receptors, these experiments were performed without addition of transferrin (Tf) or epidermal growth factor (EGF) to maintain a substantial pool of receptor molecules on the plasma membrane.

One of our objectives was to test the utility of PATagRFP in experiments for which it will prove useful, such as monitoring the dynamics of two different single molecules in the same cell, monitoring wild type and mutant molecules in the same cell, or monitoring molecules relative to distinct domains in the same cell. For example, our comparison of EGFR and VSVG puncta showed little localization with each other in the PALM images, and the tracks from sptPALM analysis suggested that, even in seemingly colocalized domains, the molecules were not present at the same time. Imaging with PAGFP-CLC showed that both the TfR and EGFR molecules could be found in distinct domains where pits were located. Plots of the molecule tracks over time confirmed that ~3% and ~4.5% of TfR and EGFR molecules, respectively, were diffusing in the same area of the plasma membrane at the same time as the pits were present. On the other hand, less than 1% of VSVG tracks were found within such domains. Thus, even in the absence of ligand activation, our data suggest that a small percentage of TfR

and EGFR molecules sample the CLC plasma membrane domains continuously whereas VSVG molecules lacking a targeting sequence rarely accessed these regions. Different color conventional fluorescent proteins may also be used for these experiments, but maintaining the molecular density low enough to image single molecules limits the number of molecules per cell. An advantage with the sptPALM approach using PATagRFP coupled with a green PAFP is that hundreds or thousands of two different chimeras are easily imaged per cell, which can provide insight into multiple molecular environments.

## 5. Summary

Compared to the best available photoactivatable dark-to-red PAmCherry1 protein, the monomeric PATagRFP variant has several substantial advantages including better pH stability, 3-fold higher brightness, and better photostability in both ensemble and single-molecule modes. The external mutations resulting in the true monomeric state of PATagRFP can be also used for TagRFP and mKate proteins to address their tendency to form weak dimers. These properties make PATagRFP an excellent protein tag for both conventional diffraction-limited microscopy and super-resolution imaging techniques. Because PATagRFP lacks a green emission state observed in green-to-red PAFPs, it allows for a greater flexibility in one-color PALM experiments and, importantly, enables a two-color sptPALM imaging. Moreover, because absorbance of the dark state of PATagRFP is ~50 nm blue-shifted comparing to that of PAmCherry1, PATagRFP exhibits 3.5-fold lower efficiency of photoactivation with blue light. That provides additional advantage for two-color sptPALM experiments, in which green PAFP such as PAGFP is imaged using standard 488 nm laser. Thus, PATagRFP addresses several disadvantages exhibited by other monomeric red PAFPs and is the photoactivatable probe of choice for super-resolution sptPALM of live cells.

## Supplementary Material

Refer to Web version on PubMed Central for supplementary material.

## Acknowledgments

## REFERENCES

1. Betzig E, Patterson GH, Sougrat R, Lindwasser OW, Olenych S, Bonifacino JS, Davidson MW, Lippincott-Schwartz J, Hess HF. Science 2006;313:1642–1645. [PubMed: 16902090]

2. Hess ST, Girirajan TP, Mason MD. Biophys. J 2006;91:4258–4272. [PubMed: 16980368]

3. Rust MJ, Bates M, Zhuang X. Nat. Methods 2006;3:793–795. [PubMed: 16896339]

4. Egner A, Geisler C, von Middendorff C, Bock H, Wenzel D, Medda R, Andresen M, Stiel AC, Jakobs S, Eggeling C, Schonle A, Hell SW. Biophys. J 2007;93:3285–3290. [PubMed: 17660318]

5. Flors C, Hotta J, Uji-i H, Dedecker P, Ando R, Mizuno H, Miyawaki A, Hofkens J. J. Am. Chem. Soc 2007;129:13970–13977. [PubMed: 17956094]

6. Lukyanov KA, Chudakov DM, Lukyanov S, Verkhusha VV. Nat. Rev. Mol. Cell Biol 2005;6:885–891. [PubMed: 16167053]

7. Manley S, Gillette JM, Patterson GH, Shroff H, Hess HF, Betzig E, Lippincott-Schwartz J. Nat. Methods 2008;5:155–157. [PubMed: 18193054]

8. Lippincott-Schwartz J, Patterson GH. Trends Cell Biol 2009;19:555–565. [PubMed: 19836954]

9. Chudakov DM, Belousov VV, Zaraisky AG, Novoselov VV, Staroverov DB, Zorov DB, Lukyanov S, Lukyanov KA. Nat. Biotechnol 2003;21:191–194. [PubMed: 12524551]

10. Ando R, Hama H, Yamamoto-Hino M, Mizuno H, Miyawaki A. Proc. Natl. Acad. Sci. U.S.A 2002;99:12651–12656. [PubMed: 12271129]

11. Wiedenmann J, Ivanchenko S, Oswald F, Schmitt F, Rocker C, Salih A, Spindler KD, Nienhaus GU. Proc. Natl. Acad. Sci. U.S.A 2004;101:15905–15910. [PubMed: 15505211]

12. Adam V, Lelimousin M, Boehme S, Desfonds G, Nienhaus K, Field MJ, Wiedenmann J, McSweeney S, Nienhaus GU, Bourgeois D. Proc. Natl. Acad. Sci. U.S.A 2008;105:18343–18348. [PubMed: 19017808]

13. Gurskaya NG, Verkhusha VV, Shcheglov AS, Staroverov DB, Chepurnykh TV, Fradkov AF, Lukyanov S, Lukyanov KA. Nat. Biotechnol 2006;24:461–465. [PubMed: 16550175]

14. Nienhaus GU, Nienhaus K, Holzle A, Ivanchenko S, Renzi F, Oswald F, Wolff M, Schmitt F, Rocker C, Vallone B, Weidemann W, Heilker R, Nar H, Wiedenmann J. Photochem. Photobiol 2006;82:351–358. [PubMed: 16613485]

15. McKinney SA, Murphy CS, Hazelwood KL, Davidson MW, Looger LL. Nat. Methods 2009;6:131–133. [PubMed: 19169260]

16. Patterson GH, Lippincott-Schwartz J. Science 2002;297:1873–1877. [PubMed: 12228718]

17. Chudakov DM, Verkhusha VV, Staroverov DB, Souslova EA, Lukyanov S, Lukyanov KA. Nat. Biotechnol 2004;22:1435–1439. [PubMed: 15502815]

18. Henderson JN, Ai HW, Campbell RE, Remington SJ. Proc. Natl. Acad. Sci. U.S.A 2007;104:6672–6677. [PubMed: 17420458]

19. Ando R, Mizuno H, Miyawaki A. Science 2004;306:1370–1373. [PubMed: 15550670]

20. Stiel AC, Andresen M, Bock H, Hilbert M, Schilde J, Schonle A, Eggeling C, Egner A, Hell SW, Jakobs S. Biophys. J 2008;95:2989–2997. [PubMed: 18658221]

21. Verkhusha VV, Sorkin A. Chem. Biol 2005;12:279–285. [PubMed: 15797211]

22. Subach FV, Patterson GH, Manley S, Gillette JM, Lippincott-Schwartz J, Verkhusha VV. Nat. Methods 2009;6:153–159. [PubMed: 19169259]

23. Merzlyak EM, Goedhart J, Shcherbo D, Bulina ME, Shcheglov AS, Fradkov AF, Gaintzeva A, Lukyanov KA, Lukyanov S, Gadella TW, Chudakov DM. Nat. Methods 2007;4:555–557. [PubMed: 17572680]

24. Ho SN, Hunt HD, Horton RM, Pullen JK, Pease LR. Gene 1989;77:51–59. [PubMed: 2744487]

25. Karstens T, Kobs K. J. Phys. Chem 1980;84:1871–1872.

26. Galperin E, Verkhusha VV, Sorkin A. Nat. Methods 2004;1:209–217. [PubMed: 15782196]

27. Shroff H, Galbraith CG, Galbraith JA, White H, Gillette J, Olenych S, Davidson MW, Betzig E. Proc. Natl. Acad. Sci. U.S.A 2007;104:20308–20313. [PubMed: 18077327]

28. Pletnev S, Shcherbo D, Chudakov DM, Pletneva N, Merzlyak EM, Wlodawer A, Dauter Z, Pletnev V. J. Biol. Chem 2008;283:28980–28987. [PubMed: 18682399]

29. Campbell RE, Tour O, Palmer AE, Steinbach PA, Baird GS, Zacharias DA, Tsien RY. Proc. Natl. Acad. Sci. U.S.A 2002;99:7877–7882. [PubMed: 12060735]

30. Shaner NC, Campbell RE, Steinbach PA, Giepmans BN, Palmer AE, Tsien RY. Nat. Biotechnol 2004;22:1567–1572. [PubMed: 15558047]

31. Shcherbo D, Merzlyak EM, Chepurnykh TV, Fradkov AF, Ermakova GV, Solovieva EA, Lukyanov KA, Bogdanova EA, Zaraisky AG, Lukyanov S, Chudakov DM. Nat. Methods 2007;4:741–746. [PubMed: 17721542]

32. Gallione CJ, Rose JK. J. Virol 1985;54:374–382. [PubMed: 2985803]

33. Sorkin A, McClure M, Huang F, Carter R. Curr. Biol 2000;10:1395–1398. [PubMed: 11084343]

34. Huebers HA, Huebers E, Josephson B, Csiba E. Biochim. Biophys. Acta 1989;991:30–35. [PubMed: 2713419]

35. Kirchhausen T. Annu. Rev. Biochem 2000;69:699–727. [PubMed: 10966473]

36. Bonifacino JS, Traub LM. Annu. Rev. Biochem 2003;72:395–447. [PubMed: 12651740]

37. Thomas DC, Brewer CB, Roth MG. J. Biol. Chem 1993;268:3313–3320. [PubMed: 8381425]

38. Baird GS, Zacharias DA, Tsien RY. Proc. Natl. Acad. Sci. U.S.A 2000;97:11984–11989. [PubMed: 11050229]

39. Subach FV, Subach OM, Gundorov IS, Morozova KS, Piatkevich KD, Cuervo AM, Verkhusha VV. Nat. Chem. Biol 2009;5:118–126. [PubMed: 19136976]

40. Prescott M, Ling M, Beddoe T, Oakley AJ, Dove S, Hoegh-Guldberg O, Devenish RJ, Rossjohn J. Structure 2003;11:275–284. [PubMed: 12623015]

41. Kogure T, Karasawa S, Araki T, Saito K, Kinjo M, Miyawaki A. Nat. Biotechnol 2006;24:577–581. [PubMed: 16648840]

42. Subach FV, Malashkevich VN, Zencheck WD, Xiao H, Filonov GS, Almo SC, Verkhusha VV. Proc. Natl. Acad. Sci. U.S.A 2009;106:21097–21102. [PubMed: 19934036]

43. Yarbrough D, Wachter RM, Kallio K, Matz MV, Remington SJ. Proc. Natl. Acad. Sci. U.S.A 2001;98:462–467. [PubMed: 11209050]

44. Subach OM, Gundorov IS, Yoshimura M, Subach FV, Zhang J, Gruenwald D, Souslova EA, Chudakov DM, Verkhusha VV. Chem. Biol 2008;15:1116–1124. [PubMed: 18940671]

45. Piatkevich KD, Verkhusha VV. Curr. Opin. Chem. Biol 2010;14:23–29. [PubMed: 19914857]

46. Shu X, Shaner NC, Yarbrough CA, Tsien RY, Remington SJ. Biochemistry 2006;45:9639–9647. [PubMed: 16893165]

47. Tubbs JL, Tainer JA, Getzoff ED. Biochemistry 2005;44:9833–9840. [PubMed: 16026155]

48. Pouwels LJ, Zhang L, Chan NH, Dorrestein PC, Wachter RM. Biochemistry 2008;47:10111–10122. [PubMed: 18759496]

49. Barondeau DP, Kassmann CJ, Tainer JA, Getzoff ED. J. Am. Chem. Soc 2007;129:3118–3126. [PubMed: 17326633]

```
                    10        20        30        40        50
                    |         |         |         |         |
GFP                 MSKGEELFTGVVPILVELDGDVNGHKFSVSGEGEGDATYGKLTLKFICTTG-KLPVP--WP
PAmCherry1  MVSKGEEDNMAIIKEFMRFKVHMEGSVNGHVFEIEGEGEGRPYEGTQTAKLKVT--KGGPLPFTWD
TagRFP          MVSKGEELIKENMHMKLYMEGTVNNHHFKCTSEGEGKPYEGTQTMRIKVV--EGGPLPFAFD
PATagRFP1297       MSELIKENMHMKLYMEGTVNNHHFKCTSEGEGKPYEGTQTMRIKVV--EGGPLPFAFD
PATagRFP1314       MSELIKENMHMKLYMEGTVNNHHFKCTSEGEGKPYEGTQTMRIKVV--EGGPLPFAFD
PATagRFP           MSELIKENMHMKLYMEGTVNNHHFKCTSEGEGKPYEGTQTMRIKVV--EGGPLPFAFD


                    60        70        80        90        100       110
                    |          ***   |            |         |         |
GFP                 TLVTTFSYGVQCFSRYPDHMKQHDFFKSAMPEGYVQERTIFFKDDGNYKTRAEVKFEGDT
PAmCherry1          ILSPQFMYGSNAYVKHPADIP--DYFKLSFPEGFKWERVMKFEDGGVVTVTQDSSLQDGE
TagRFP              ILATSFMYGSRTFINHTQGIP--DFFKQSFPEGFTWERVTTYEDGGVLTATQDTSLQDGC
PATagRFP1297        ILATSFMYGSSTFINHTQGIP--DFWKQSFPEGFTWERVTTYEDGGVLTATQDTSLQDGC
PATagRFP1314        ILATSFMYGSSTFINHTQGIP--DFWKQSFPEGFTWERVTTYEDGGVLTATQDTSLQDGC
PATagRFP            ILATSFMYGSSTFINHTQGIP--DFWKQSFPEGFTWERVTTYEDGGVLTATQDTSLQDGC


                    120       130       140       150       160       170
                    |         |         |         |         |         |
GFP                 LVNRIELKGIDFKEDGNILGHKLEYNYNSHNVYIMADKQKNGIKVNFKIRHNIEDGSVQL
PAmCherry1          FIYKVKLRGTNFPSDGPVM-QKKTMGWEALSERMYP--EDGALKGEVKPRVKLKDGGHYD
TagRFP              LIYNVKIRGVNFPSNGPVM-QKKTLGWEANTEMLYP--ADGGLEGRSDMALKLVGGGHLI
PATagRFP1297        LIYNVKIRGVNFPSNGPVM-KKKTLGWEPSTEMLYP--ADGGLGGVVDMALKLVGGGHLI
PATagRFP1314        LIYNVKIRGVNFPSNGPVM-KKKTLGWEPSTEMLYP--ADGGLEGVVNMALKLVGGGHLI
PATagRFP            LIYNVKIRGVNFPSNGPVM-KKKTLGWEPSTEKLKP--ADGGLEGRVDMALKLVGGGHLI


                    180       190       200       210       220       230
                    |         |         |         |         |         |
GFP                 ADHYQQNTPIGD-GPVLLPDNHYLSTQSALSKDPNEKRDHMVLLEFVTAAGITHGMDELYK
PAGFP               ADHYQQNTPIGD-GPVLLPDNHYLSHQSALSKDPNEKRDHMVLLEFVTAAGITLGMDELYK
PAmCherry1          AEVKTTYKAKK---PVQLPGAYNVNRKLDITSHNEDYT-IVEQYERAEGRHSTGGMDELYK
TagRFP              CNFKTTYRSKKPAKNLKMPGVYYVDHRLERIKE-ADKETYVEQHEVAVARYCDLPSKLGHKLN
PATagRFP1297        CNFKTTYRSKKPAKNLKMPGVYYVDRRLEIIKE-ADKETYWEQHEVAVARYCDLPSKLGHKLN
PATagRFP1314        CNFKTTYRSKKPAKNLKMPGVYYVDRRLEQIKE-ADKETYWEQHEVAVARYCDLPSKLGHKLN
PATagRFP            CNFKTTYRSKKPAKNLKMPGVYYVDRRLEIIKE-ADKETYWEQHEVAVARYSDLPSKLGHKLN
```
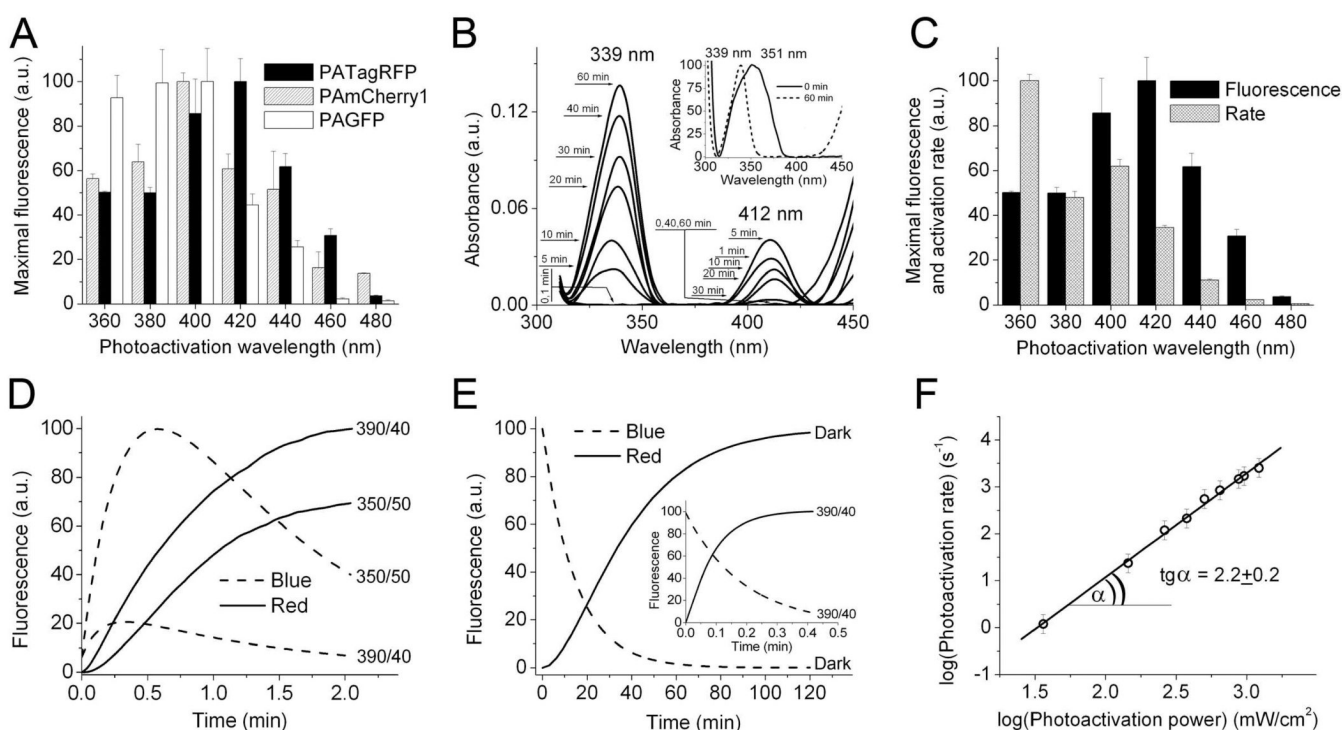
**Figure 1.**
Alignment of amino acid sequences for the PATagRFP variants. Alignment numbering follows that of *Aequorea victoria* GFP. Residues buried in the protein β-barrel fold are shaded. Asterisks indicate residues that form the chromophore. Mutations resulted in the conversion of TagRFP into the photoactivatable PATagRFP variants are shown in white on the black background.
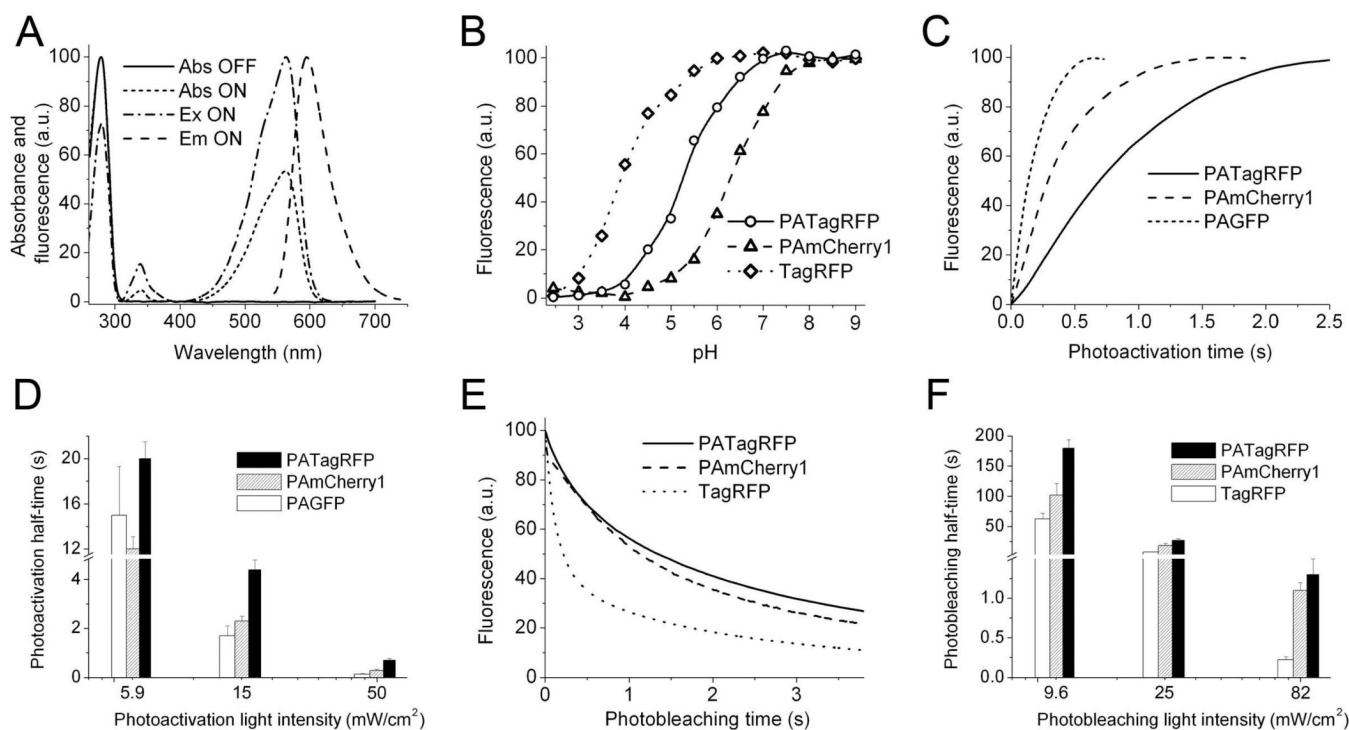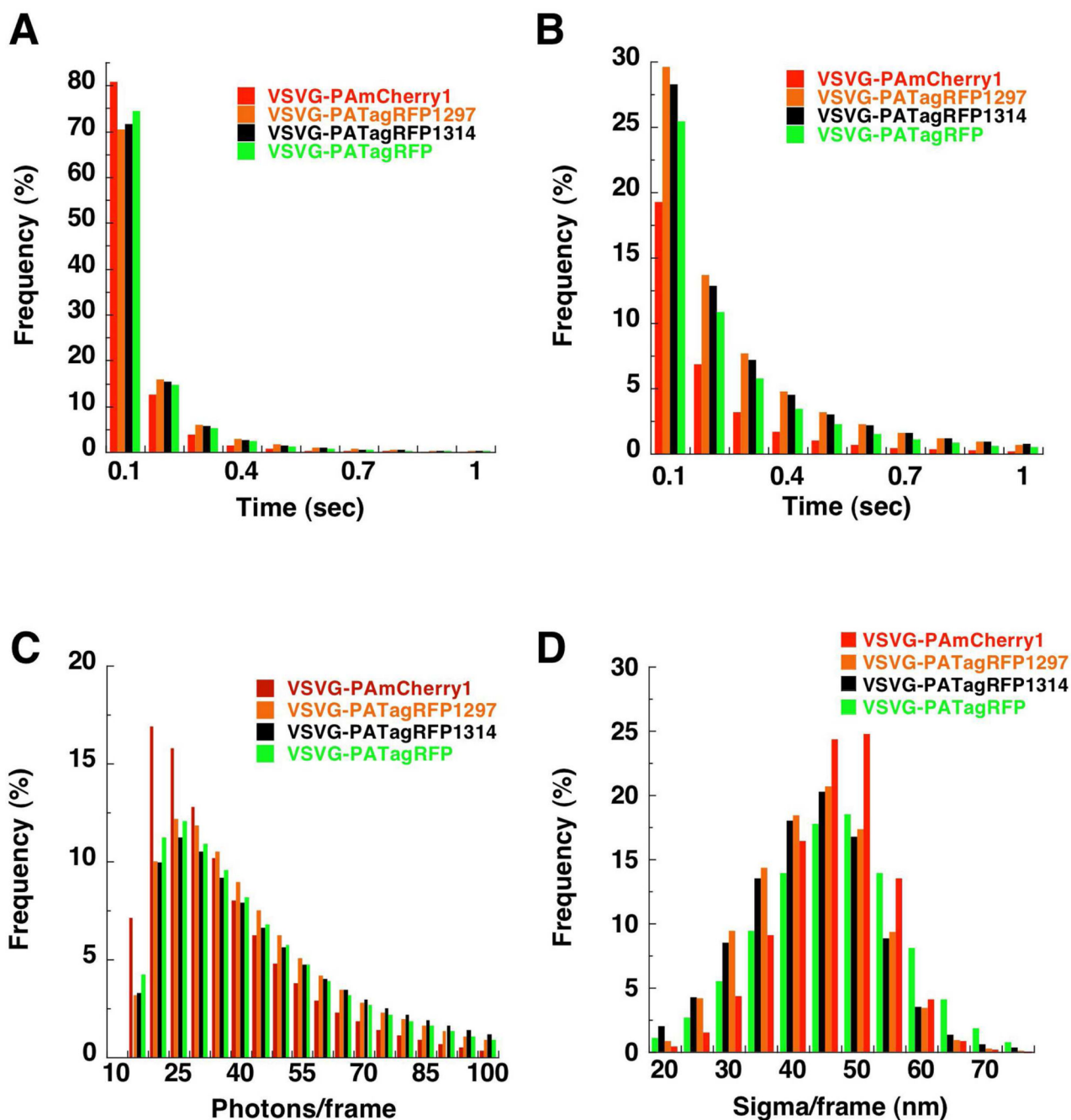
**Figure 2.**
Spectral and biochemical properties of the purified PATagRFP protein at room temperature.
(A) Absorbance spectrum before the photoactivation with 399 nm laser line (solid line), and
absorbance (dot line), excitation (dashed dot line) and emission (dashed line) spectra after. (B)
Equilibrium pH dependence for the fluorescence of PATagRFP (circles), PAmCherry1
(triangles) and TagRFP (diamonds). (C) Photoactivation kinetics for PATagRFP (solid line),
PAmCherry1 (dashed line) and PAGRFP (dot line) at 50 mW/cm$^2$ at the back of the 100× oil
objective lens. (D) Photoactivation half-times for PATagRFP (solid columns), PAmCherry1
(dashed columns) and PAGFP (open columns) at different power densities. (E) Photobleaching
kinetics for PATagRFP (solid line), PAmCherry1 (dashed line) and TagRFP (dot line) at 82
mW/cm$^2$. (F) Photobleaching half-times for PATagRFP (solid columns), PAmCherry1 (dashed
columns) and TagRFP (open columns) at different power densities. In (C–F) protein properties
were measured in aqueous drops in oil using an Olympus IX-81 inverted microscope equipped
with 200 W metal-halide lamp, 100× oil objective lens, and 390/40 nm (C, D) or 570/30 nm
(E, F) filters. The power densities were measured at a rear aperture of the objective lens. The
photobleaching data (E, F) were normalized to the spectral output of the lamp, transmission
profile of the filter and dichroic mirror, and absorbance spectra of the proteins.

**Figure 3.**
Photoactivation characteristics of the purified PATagRFP protein at room temperature. (A) Maximal fluorescence intensity for PATagRFP (solid columns), PAmCherry1 (dashed columns) and PAGFP (open columns) achieved at different photoactivation wavelengths. (B) Changes of the PATagRFP absorbance during photoactivation with a 405/15 nm LED array providing 50 mW/cm$^2$ in a cuvette with the protein. Insert shows the absorbance of the PATagRFP sample (27 mg/ml) at the beginning (solid line) and after 60 min (dashed line) of the photoactivation, normalized to 100%. (C) Spectral dependence of the maximal fluorescence intensity (solid columns) compared to the maximal photoactivation rate (dashed columns) for PATagRFP. The maximal values of the photoactivation rates were normalized to the light power in each wavelength band. In (A, C) protein samples were studied in aqueous drops in oil using Olympus IX-81 inverted microscope equipped with monochromator having 20 nm bandwidth, 150 W xenon lamp, and 100× oil objective lens. (D) Time courses of the blue (dashed line) and red (solid line) forms of PATagRFP during photoactivation with either 350/50 nm or 390/40 nm light at the same power density of 50 mW/cm$^2$ at a rear aperture of the 100× oil objective lens. The kinetics was measured in aqueous drops in oil using an Olympus IX-81 inverted microscope equipped with 200 W metal-halide lamp. (E) Time courses of the blue (dashed line) and red (solid line) forms of PATagRFP, which was pre-activated for 1 min using the conditions in (D) with 350/50 nm light, in the darkness. Low intensity probing light of a Fluoromax-3 fluorometer was used. The blue and red fluorescence intensities of a pre-activated PATagRFP were normalized to initial 100% and 0%, respectively. Insert shows time courses of the same forms of the similarly pre-activated PATagRFP but during its illumination with 390/40 nm light using the conditions in (D). (F) Dependence of the PATagRFP maximal photoactivation rate on the photoactivation power of 350/50 nm light. Other conditions are similar to those for (D).
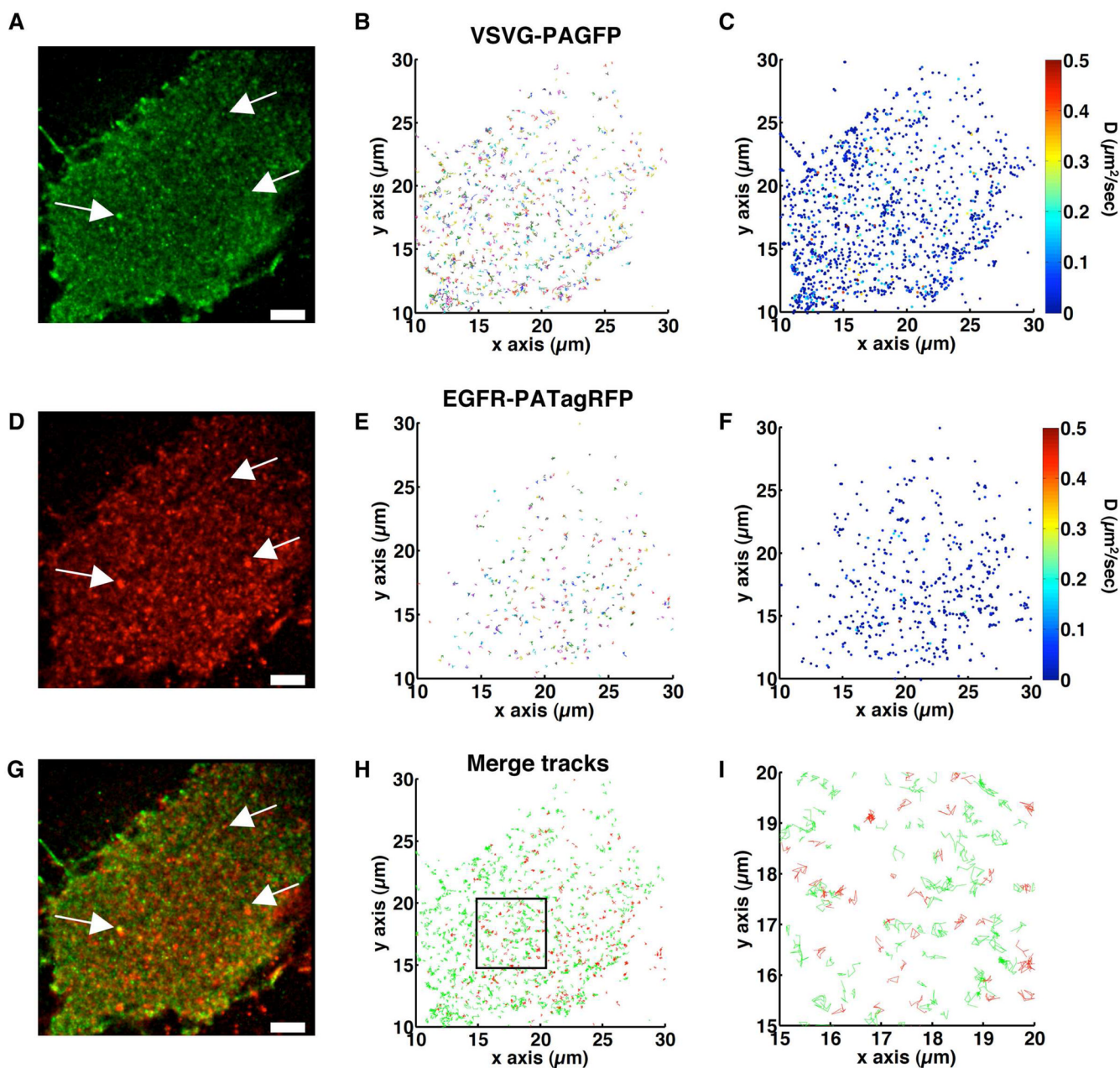
**Figure 4.**
sptPALM imaging of VSVG chimeras: single molecule duration. (A) Duration of molecule fluorescence in 0.106 second images is displayed as a histogram for VSVG-PAmCherry1, VSVG-PATagRFP1297, VSVG-PATagRFP1314, and VSVG-PATagRFP. (B) Data in (A) is redisplayed as a histogram indicating the percentage of total molecules that last longer than the time shown on the X-axis. (C) Distribution of the number of photons during 0.106 second frames collected from molecules in cells expressing VSVG-PAmCherry1 (mean, 42.4; median, 33), VSVG-PATagRFP1297 (mean, 52.4; median, 41), VSVG-PATagRFP1314 (mean, 60.4; median, 43), and VSVG-PATagRFP (mean, 60.8; median, 41). (D) Distribution of σ in cells expressing VSVG-PAmCherry1 (mean, 48.1; median, 48.8), VSVG-PATagRFP1297 (mean,

45.2; median, 45.6), VSVG-PATagRFP1314 (mean, 45.1; median, 45.5), and VSVG-PATagRFP (mean, 48.9; median, 49.4).
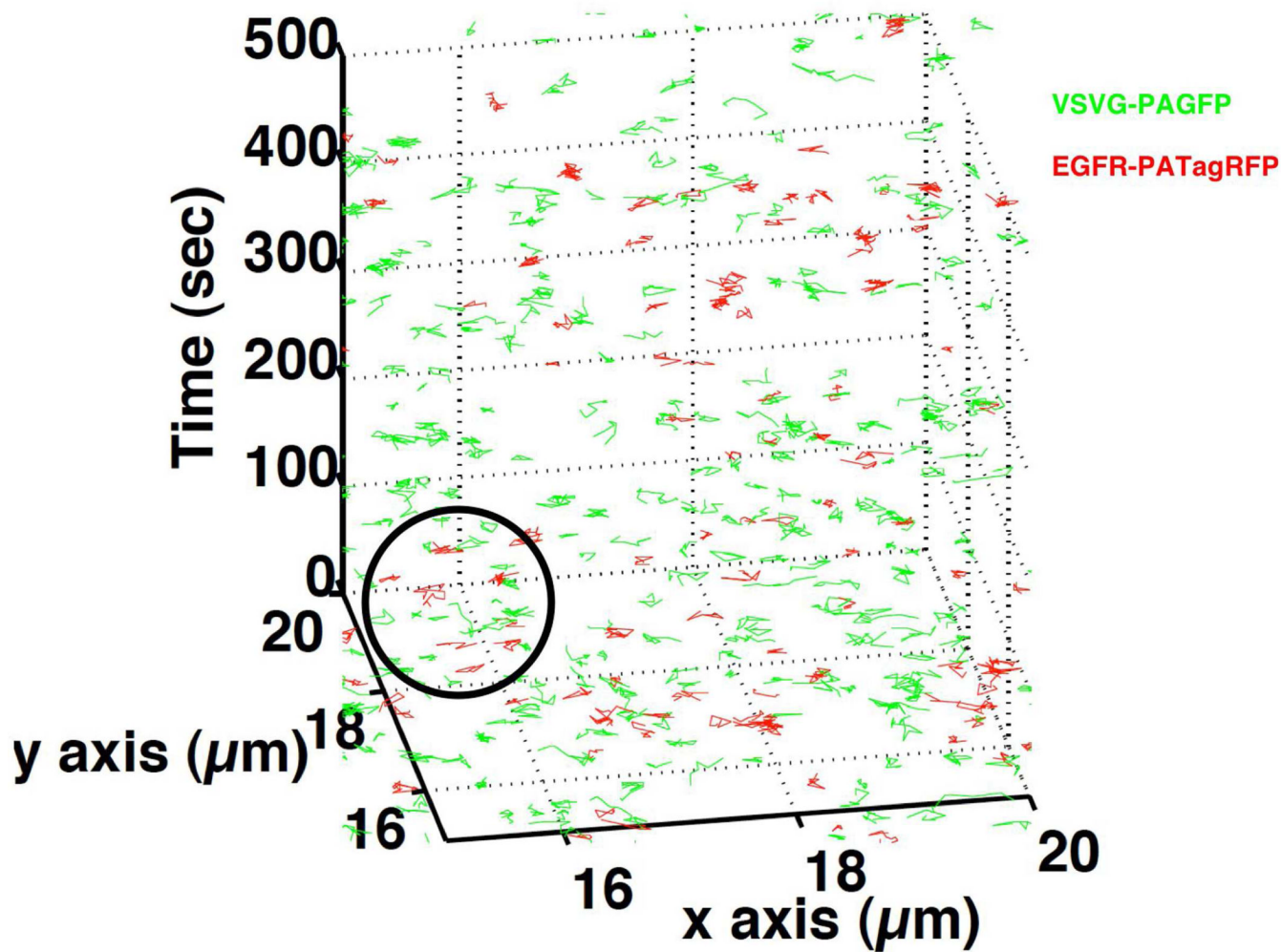
**Figure 5.**
Two-color sptPALM of VSVG-PAGFP and EGFR-PATagRFP. (A–C) VSVG-PAGFP and (D–F) EGFR-PATagRFP were expressed in COS-7 cells and imaged by TIRF microscopy at 9.4 frames/sec under low levels of 561 nm excitation (<60 W/cm$^2$) and 405 nm photoactivation (<2.5 W/cm$^2$) at ~37°C. PALM analysis was performed as previously published.1 PALM images of (A) VSVG-PAGFP (green) and (D) EGFR-PATagRFP (red) are merged (G) to show the relative distributions of the molecules. Arrows indicate areas of apparent colocalization between the VSVG and EGFR molecules. Scale bars are 2 μm. sptPALM analyses were performed as previously published.7 Tracks of (B) VSVG-PAGFP and (E) EGFR-PATagRFP molecules lasting longer than 0.7 sec are plotted with each track represented by a different color. Mean squared displacements and diffusion coefficients were determined as previously published.7 Diffusion coefficients are plotted for (C) VSVG-PAGFP and (D) EGFR-

PATagRFP molecules at the start of the tracks and color coded according to the color maps at the right. (H) VSVG-PAGFP (green) and EGFR-PATagRFP (red) tracks are merged. (I) A zoomed view of the region indicated by the square in (H). Approximately 1635 VSVG molecules were tracked along with 627 EGFR-PATagRFP molecules.

**Figure 6.**
Three dimensional plot of VSVG-PAGFP and EGFR-PATagRFP two-color sptPALM. The X-Y tracks of VSVG-PAGFP and EGFR-PATagRFP from Figure 5I are plotted as a function of time in the Z-axis. The black circle outlines the region that indicated overlapping tracks in Figure 5I.
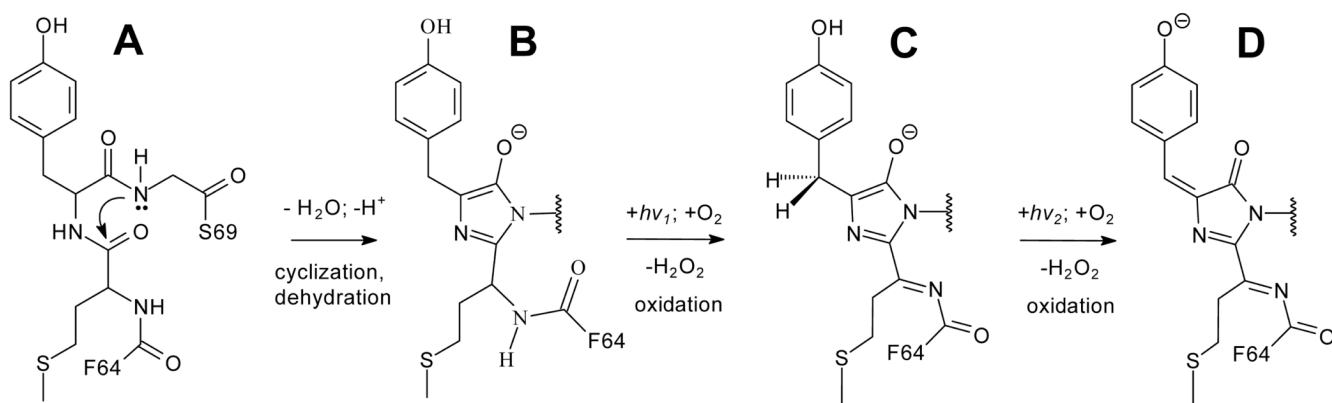
**Scheme 1.**
Suggested mechanism for the PATagRFP photoactivation. The intact polypeptide (A) undergoes a backbone cyclization followed by a dehydration of its 5-membered ring with a formation of the aromatic α-enolate (B) absorbing at 351 nm. Absorption of the first photon ($hv_1$) induces an oxidation of the N-C$^\alpha$ bond to N-acylimine that, in turn, produces the chromophore moiety (C), in which the π-electron system is delocalized over the imidazolone and N-acylimine groups of the chromophore and carbonyl of Phe65. Further absorption of the second photon ($hv_2$) results in an oxidation of the C$^\alpha$-C$^\beta$ bond of Tyr66 with a formation of the red fluorescent chromophore of PATagRFP (D). The $hv_1$ and $hv_2$ symbols denote the illumination with 351 nm and 412 nm light, respectively.

**Table 1**

Ensemble characteristics of the PATagRFP variants after photoactivation compared to other currently available monomeric photoactivatable red FPs and to parental TagRFP.

| Protein | PATagRFP1297 | PATagRFP1314 | PATagRFP | PAmCherry1 | tdEosFP | mEos2 | Dendra2 | TagRFP |
|---|---|---|---|---|---|---|---|---|
| Type of photoconversion | dark to red | dark to red | dark to red | dark to red | green to red | green to red | green to red | none |
| Absorbance peak (nm) | 563 | 562 | 562 | 564 | 569 | 573 | 553 | 555 |
| Extinction coefficient ($M^{-1}cm^{-1}$) | 63,000 | 61,000 | 66,000 | 18,000 | (33,000) 30,000 | (46,000) | (35,000) | (100,000) 132,000 |
| Emission peak (nm) | 595 | 596 | 595 | 595 | 582 | 584 | 573 | 584 |
| Quantum yield | 0.42 | 0.46 | 0.38 | 0.46 | (0.60) | (0.66) | (0.55) | (0.48) 0.30 |
| Brightness relative to TagRFP (%) | 67 | 71 | 63 | 21 | 46 | (76) | (49) | 100 |
| p$Ka$ | ND | ND | 5.3 | 6.3 | 6.7 | (6.4) | (6.9) | 3.9 |
| Maturation half-time at 37°C (min) | 25 | 25 | 75 | ND | ND | ND | (90) | 90 |
| Photobleaching half-time (s) * | 81 | 83 | 180 | 102 | ND | ND | ND | 63 |
| Oligomeric state | monomer-dimer-tetramer | monomer-dimer | monomer | monomer | (tandem-dimer) | (monomer-dimer) | (monomer) | monomer-dimer |

tdEosFP, mEos2, Dendra2 and TagRFP characteristics are presented from the original papers (shown in brackets) or measured in our laboratory using the same conditions as for the PATagRFP variants.

*
Determined at 9.6 mW/cm$^2$ at a rear aperture of the 100× 1.4 NA oil objective lens. ND, not determined.